Imaging the quantal substructure of single IP$_3$R channel activity during Ca^{2+} puffs in intact mammalian cells

Ian F. Smith[a,1] and Ian Parker[a,b]

Departments of [a]Neurobiology and Behavior and [b]Physiology and Biophysics, University of California at Irvine, Irvine, CA 92697-4550

The spatiotemporal patterning of Ca^{2+} signals regulates numerous cellular functions, and is determined by the functional properties and spatial clustering of inositol trisphosphate receptor (IP$_3$R) Ca^{2+} release channels in the endoplasmic reticulum membrane. However, studies at the single-channel level have been hampered because IP$_3$Rs are inaccessible to patch-clamp recording in intact cells, and because excised organelle and bilayer reconstitution systems disrupt the Ca^{2+}-induced Ca^{2+} release (CICR) process that mediates channel-channel coordination. We introduce here the use of total internal reflection fluorescence microscopy to image single-channel Ca^{2+} flux through individual and clustered IP$_3$Rs in intact mammalian cells. This enables a quantal dissection of the local calcium puffs that constitute building blocks of cellular Ca^{2+} signals, revealing stochastic recruitment of, on average, approximately 6 active IP$_3$Rs clustered within <500 nm. Channel openings are rapidly ($\approx$10 ms) recruited by opening of an initial trigger channel, and a similarly rapid inhibitory process terminates puffs despite local [Ca^{2+}] elevation that would otherwise sustain Ca^{2+}-induced Ca^{2+} release indefinitely. Minimally invasive, nano-scale Ca^{2+} imaging provides a powerful tool for the functional study of intracellular Ca^{2+} release channels while maintaining the native architecture and dynamic interactions essential for discrete and selective cell signaling.

calcium signaling | single-channel flux | TIRF microscopy | optical patch-clamp

Cytosolic signals resulting from Ca^{2+} liberation from the endoplasmic reticulum (ER) through inositol trisphosphate receptor/channels (IP$_3$Rs) regulate cellular functions as diverse as gene expression, secretion, and synaptic plasticity (1). Information is encoded by the spatiotemporal patterning of cytosolic Ca^{2+} transients, which are organized in a hierarchical manner resulting from the clustering of IP$_3$R in the ER membrane. Local, "elementary" Ca^{2+} transients (i.e., Ca^{2+} puffs) are generated by the concerted openings of multiple IP$_3$Rs within a cluster, and serve autonomous signaling functions as well as constituting the building blocks from which global cellular Ca^{2+} waves are constructed (2–6). In turn, puffs are composed from "fundamental" signals (i.e., Ca^{2+} blips), representing Ca^{2+} flux through individual IP$_3$Rs (7–10). Information concerning the spatial localization and numbers of IP$_3$Rs involved in a puff, and the mechanisms and kinetics by which their activity is coordinated, is essential to understand how these channels act to initiate and terminate local Ca^{2+} liberation (11). However, studies at the single-channel level have been hampered because the intracellular location of IP$_3$Rs renders them inaccessible to patch-clamp recording within intact cells. Electrophysiological recordings have thus been restricted to excised nuclei or lipid bilayer reconstitution systems (11), approaches that provide little or no spatial information and disrupt the process of Ca^{2+}-induced Ca^{2+} release (CICR) that mediates channel-channel interactions (12).

Our knowledge of local cellular Ca^{2+} signaling instead derives largely from minimally invasive whole-cell Ca^{2+} imaging techniques. Nonetheless, recordings by conventional wide-field or confocal fluorescence microscopy fail to provide resolution at the single-channel level, and puffs imaged by these techniques show an apparently monotonic rising phase lasting tens of milliseconds as Ca^{2+} is liberated through open channels, followed by a slower decay as the Ca^{2+} micro-domain at the puff site dissipates following channel closure (4–6). Although specific instances of single IP$_3$R channel fluorescence signals have been reported as isolated blips (7, 13) and as "trigger" events immediately preceding puffs (10), it had not been possible to directly dissect the contributions of individual channels during puffs. Here, we capitalize on experimental and theoretical findings that the resolution of local Ca^{2+} signals can be dramatically improved by monitoring fluorescence from attoliter volumes around open channels by means of total internal reflection fluorescence (TIRF) microscopy (14). We had previously used this approach to image single-channel calcium fluorescence transients arising from gating of Ca^{2+}-permeable channels in the plasma membrane (15, 16). Following the discovery that a population of puff sites in SH-SY5Y neuroblastoma cells lie sufficiently close to the plasma membrane to be within range of the approximately 100-nm evanescent field of the TIRF microscope (17), we now apply this technique to resolve the properties of individual intracellular IP$_3$R channels, and to dissect their contributions during Ca^{2+} puffs within intact mammalian cells.

Results

Resolving Ca^{2+} Fluorescence Signals from Individual IP$_3$Rs. We loaded SH-SY5Y cells with fluo-4 and caged iIP$_3$ by incubation with membrane-permeant esters, and imaged local Ca^{2+} puffs evoked by photo-released i-IP$_3$. Puffs imaged by wide-field epifluorescence showed smoothly rising and falling phases (Fig. 1*A*, gray trace), on which it was not possible to resolve the underlying step-wise changes that would be expected as individual channels stochastically open and close. To then achieve single-channel resolution, we used TIRF imaging of a subset of puff sites located close to the plasma membrane (17), so that rapid binding of Ca^{2+} to the fast indicator dye within attoliter cytosolic volumes around puff sites yields fluorescence signals that more closely track instantaneous Ca^{2+} flux through IP$_3$R channels (14). Additionally, we gained a further improvement by loading cells with EGTA, a Ca^{2+} buffer that inhibits wave propagation (17–19) and accelerates the collapse of the local Ca^{2+} micro-domain but, because of its slow binding kinetics, minimally perturbs local free [Ca^{2+}] within a cluster (14) and has little effect on peak puff amplitudes (17–19). EGTA is thus

Fig. 1. Imaging IP$_3$-evoked Ca^{2+} liberation with single-channel resolution. (*A*) Comparison of representative puffs recorded in SH-SY5Y cells following photo-release of i-IP$_3$ using wide-field fluorescence microscopy (gray trace) and TIRF microscopy together with EGTA loading (black trace). Both traces show fluorescence ratio changes (ΔF/F$_0$) averaged within 1×1 μm regions of interest centered on puff sites. (*B*) Representative image frames taken from a video sequence showing puffs evoked by photo-released iIP$_3$ at different sites in 2 SH-SY5Y cells. Cell outlines (resting fluo-4 fluorescence) are shown in gray, and transient increases in [Ca^{2+}]$_i$ are overlaid in red. (*C*) Graphical representation of puff activity evoked by photo-released iIP$_3$ (arrow) at >70 sites. Ca^{2+} transients (puffs and blips) are represented on a pseudo-color scale (''warmer'' colors indicate higher [Ca^{2+}]) as indicated by the bar. Time runs from left to right and different puff sites are depicted vertically in random order.

expected to have little effect on the coordinated openings of clustered IP$_3$R, but by "mopping up" residual Ca^{2+} ions sharpens the spatial and temporal gradients of local free [Ca^{2+}]. The resulting enhancement in resolution achieved by these combined techniques is illustrated by the black trace in Fig. 1*A*, revealing abrupt steps in fluorescence level that we interpret to reflect channel openings and closings.

Local Ca^{2+} transients were typically observed at 4 or 5 sites per cell, and activity persisted for >1 min following a photolysis flash (Figs. 1 *B* and *C* and 2*A*; Movie S1), likely because the i-IP$_3$ resulting from photolysis is degraded more slowly than native IP$_3$ (17, 20). Cells were essentially quiescent before photo-release of i-IP$_3$, and after stimulation puffs continued for >60 s in the absence of extracellular Ca^{2+} ($n = 7$ cells), indicating that they are evoked by intracellular Ca^{2+} liberation through IP$_3$Rs. Moreover, there appears to be little or no secondary contribution evoked by CICR through ryanodine receptors (RyRs; the other major class of Ca^{2+} release channels). In our hands, bath application of caffeine (2–25 mM), an agonist of RyR, failed to evoke detectable Ca^{2+} signals ($n = 8$ cells), and another report (21) describes caffeine-evoked signals in only a small minority (1%–8%) of SH-SY5Y cells and then only after priming by depolarization-evoked Ca^{2+} entry.

Ca^{2+} signals at individual sites were markedly heterogeneous, typically consisting of a mix of small (ΔF/F$_0$, 0.11 ± 0.01) "rectangular" signals (i.e., blips), together with larger events of widely varying sizes with amplitudes as great as an ΔF/F of ≈2 (Fig. 2*A*). Moreover, there was appreciable heterogeneity among sites, with a few (6%) showing only single-channel-like blip activity (Fig. 2*B*). The unitary blip fluorescence signals are consistent with their arising from Ca^{2+} flux through a single

Fig. 2. Puff activity recorded in SH-SY5Y cells following photo-release of i-IP$_3$ using TIRF microscopy. (*A*) Traces illustrate puffs evoked at 5 sites in different cells following flash photo-release of i-IP$_3$ when marked by the arrow. (*B*) Examples of other sites that displayed exclusively single-channel activity. (*C*) Selected examples of puffs (taken from different sites and different cells) shown on an expanded time scale, illustrating step-wise transitions in Ca^{2+} fluorescence.

IP$_3$R. The "square" appearance and apparently random occurrence of blips is reminiscent of electrophysiological (22) and optical (16) single-channel recordings; the mean duration of blips (compare with Fig. 5*A*) closely matches the mean open time of IP$_3$R channels in SH-SY5Y cells as recorded by patch clamp (as described later); and comparison of the mean fluorescence
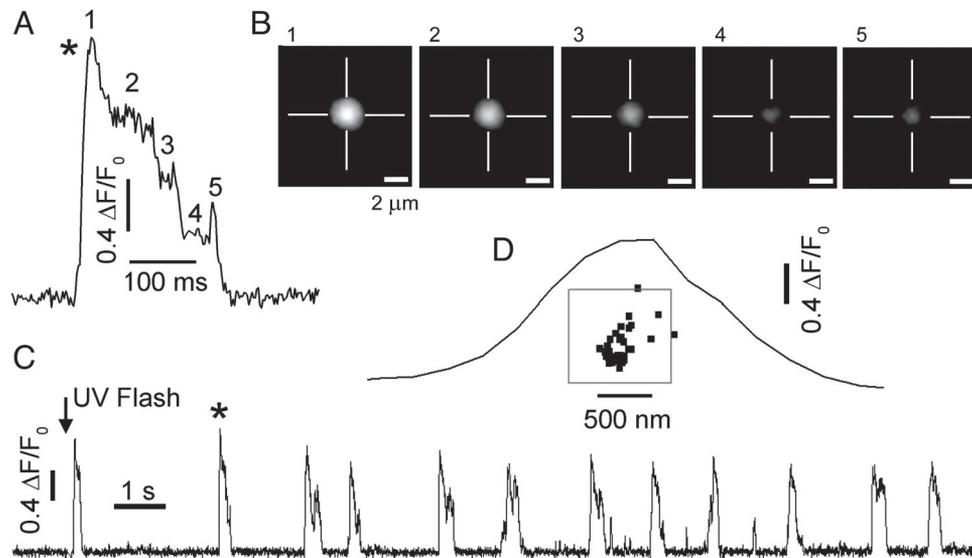
Fig. 3. Ca^{2+} sources during different amplitude steps at a puff site localize within a few hundred nanometers. (*A*) Ca^{2+} signal from a 1-μm^2 region of interest showing 5 discrete amplitude levels during a single puff. (*B*) Sequence of images showing the location of the Ca^{2+} fluorescence at times corresponding to the numbered levels in *A*. Each panel is an average of image frames captured during that step, and cross-hairs mark the centroid position of the fluorescence signal in the first frame. (*C*) Extended record showing multiple events at the same region of interest. The puff marked by the asterisk is that illustrated in *A*. (*D*) Scatter plot marks the centroid positions of Ca^{2+} signals during all (*n* = 53) step amplitude levels throughout the record in *C*, derived by fitting 2D Gaussian functions to averaged images like those in *B*. Square marks the region of interest from which the fluorescence traces in *A* and *B* were measured. The curve shows, on the same scale, the spatial distribution of fluorescence measured along a line passing through the center of the puff in *B1*.

amplitude of blips with that ($\Delta F/F_0$, ≈ 0.5) of single nicotinic receptors passing a Ca^{2+} current of approximately 0.25 pA (16) implies a Ca^{2+} current of approximately 0.05 pA, comparable to that (≈ 0.1 pA) estimated for IP_3R channels in the intact cell (11).

Quantal Analysis of Ca^{2+} Puffs. Importantly, puffs imaged by TIRF microscopy showed abrupt step-wise transitions between fluorescence levels (Fig. 2*C* and Movie S2), predominantly during their falling phase. We can exclude that these steps arose because the site of Ca^{2+} liberation shifted outside the region of interest to cause artifactually smaller fluorescence signals as Ca^{2+} became diluted by diffusion. Instead, the centroid locations of Ca^{2+}-fluorescence signals during multiple steps deviated by no more than few hundred nanometers of one another (Fig. 3 and Movie S3), a distance within the region of interest used to measure the traces, and small in comparison to the spatial spread of the fluorescence signal (Fig. 3*D*). We thus conclude that transitions in amplitude levels arise from the step-wise recruitment and closing of varying numbers of IP_3Rs, localized within clusters with dimensions of <500 nm.

This concept is further supported by a quantal analysis (23) of amplitude levels, showing a multimodal distribution with recurring peaks at integer multiples of the unitary blip amplitude (Fig. 4*A*). Although it has been proposed that local depletion of ER Ca^{2+} may result in an incrementally smaller single-channel Ca^{2+} flux as progressively greater numbers of IP_3R channels open (24), our results suggest that the fluorescence signals contributed by each channel summate linearly. Discrete peaks remain evident in the step amplitude distribution at equal increments as great as 6 or 7 times the unitary amplitude (Fig. 4*A*); analysis of step decrements from the peak of large puffs (>15 times the unitary event) did not reveal steps appreciably smaller than the unitary event (data not shown), and even the largest signals ($\Delta F/F_0$, ≈ 2) are well within the linear range of Fluo-4 (F_{max}/F_{min}, >20). We thus estimate the number of IP_3R channels open at a site at any given time simply by dividing the fluorescence signal ($\Delta F/F_0$) by the mean unitary event signal at that site.

Intra- and Inter-Site Variability in Numbers of IP_3Rs. The numbers of channels open at the peak of each event follow a highly skewed distribution, with many events involving concurrent openings of only 1 or 2 channels and progressively fewer involving as many as 20 channels (Fig. 4*B*). Much of this variability results from inter-site heterogeneity, as shown in Fig. 4*C*, plotting the amplitude distribution of the largest event seen at any given site. Because the photolysis flash typically evoked tens of events at each site, this provides an approximation of the minimal total number of functional IP_3R channels within that cluster. The mean number per site is 6.02 ± 0.48 (*n* > 80 sites), and again follows a highly skewed distribution, including a few ($\approx 6\%$) sites comprising a lone channel, a majority of sites comprising a handful of channels, and a small proportion ($\approx 16\%$) containing >10 channels. These data pool observations from many cells, but observations of widely varying maximal event amplitudes among sites within an individual cell (e.g., $\Delta F/F_0$, 0.15–2.26) indicate that the variability arises primarily from inter-site variability rather than from differences between cells. To then examine the variability among successive responses at a given site, we minimized inter-site variability by pooling data from selected sites with maximal event sizes 5 to 10 times the unitary signal. This revealed an approximately equal proportion of events involving as many as 6 channels, and decreasing numbers of larger events (Fig. 4*D*).

What might account for this wide variability in responses at a given puff site? We considered several simplified models, based on the assumption that CICR evoked by spontaneous opening of an initial channel triggers a puff by increasing the opening probability of neighboring IP_3Rs in the cluster (25). Fig. 4*E* plots the data in terms of the number of additional channels responding to this trigger. We first considered a model comprised of *n* independent channels, each of which has an equal probability *p* of being triggered. The open symbols in Fig. 4*E* shows the predicted distribution for *n* = 10, and with *P* = 0.34 so as to match the observed mean number of responding channels. This provides a poor fit to the data, and other simulations with between 8 and 50 channels similarly failed to account for the

Fig. 4. Quantal analysis of Ca²⁺ puffs. Histograms show distributions of event and step-level amplitudes derived from measurements at 87 sites in 20 cells. In all cases, the amplitudes of Ca²⁺ fluorescence signals are plotted after normalizing to the mean unitary event (blip) magnitude at each given site. (*A*) Distribution of all (*n* = 1,531) peak and step level amplitudes. The curve is a sum of 7 Gaussian distributions centered at integer multiples of the mean unitary event magnitude and with respective peak amplitudes/SDs of 151/0.22, 80/0.31, 46/0.32, 30/0.37, 17/0.35, 8/0.31, and 11/1.3. (*B*) Distribution of normalized peak amplitudes of all discrete events at all puff sites. (*C*) Distribution of amplitudes of the largest event observed at each site; providing a measure of the minimal number of functional IP₃Rs at that site. (*D*) Distribution of event amplitudes as in *B*, after selecting only those sites where the largest puff was between 5 and 10 times the unitary event amplitude so as to reduce inter-site variability. (*E*) Distribution of number of IP₃R channels activated by opening of an initial trigger channel, estimated by re-plotting the data in *D* after subtracting the initial channel. Curves show predicted distributions assuming respective models in which independent IP₃Rs have equal probability of opening (open symbols), or in which the probability of opening increases linearly with the number of already open channels (filled symbols). See text for further explanation. (*F*) Curve shows the distribution predicted by a model comprising a cluster of 10 channels, where the probability of opening increases as a cube root function of the number of already open channels. Data are reproduced from *E*.

data. We then considered schemes in which additional Ca²⁺ liberation through sequential openings of channels further increases the opening probability of remaining IP₃Rs in a cluster. A strongly cooperative model in which the opening probability increases linearly as a function of the number of already open channels yielded a markedly bi-modal distribution (closed symbols, Fig. 4*E*), comprised largely of "fizzles" in which few or no channels were triggered, and "explosions" involving successive triggering of almost all channels. Instead, we obtained a better fit to the experimental distribution by a weakly cooperative model, wherein Ca²⁺ flux through successive channels contributed a progressively smaller increase in opening probability (Fig. 4*F*; simulated empirically for *p* proportional to $n^{1/3}$). Although this model predicts a greater than observed number of failures (i.e., single-channel openings that fail to trigger further channels), this discrepancy may well arise artifactually from the difficulty in resolving these blips above the noise level.

Kinetics of IP₃R Channel Gating During Puffs. The ability to resolve channel openings and closings further allowed us to dissect the dynamics of puff initiation and termination in terms of single IP₃R channel kinetics. Blip durations largely follow a single exponential distribution (Fig. 5*A*), as expected for stochastic gating of single channels, and their time constant (≈17 ms) is comparable to the mean open dwell time observed by patch-clamp of native IP₃Rs in SH-SY5Y cell nuclei (≈13.5 ms; J.K. Foskett and D. Mak, personal communication). Exceptionally, a few sites showed appreciably longer single channel-like events (e.g., Fig. 2*B Upper*). These may reflect modal gating of IP₃Rs (26), and were excluded from analysis. Mean puff durations were 2 to 3 times longer than blips (Fig. 5*B*), and the puff termination time (from peak to baseline) increased as a less than linear function of the number of channels open at the peak (Fig. 5*C*). The relationship between puff duration and amplitude (Fig. 5*C*) and the observed distribution of puff termination times (Fig. 5*B*) are both predicted well by a statistical model in which those IP₃R channels that are open at the peak of a puff close stochastically and independently following a mean dwell time characteristic of the unitary blips.

Figs. 5 *D* and *E* show, respectively, the mean opening and closing rates of channels during selected puffs involving 5 to 10 IP₃Rs, derived by expressing the transitions in fluorescence amplitude between sequential time bins in terms of the unitary single-channel signal. The opening rate peaks at approximately 1 channel ms⁻¹ during the first 10 ms, but within 20 ms then subsides to a rate ≈40 times lower, with only infrequent openings persisting throughout the remainder of the puff (Fig. 5*D*).

Discussion

The clustered localization of intracellular Ca²⁺ release channels such as IP₃R and RyR, in conjunction with their coordination by Ca²⁺ diffusion and CICR, underlie the spatiotemporal patterning of intracellular Ca²⁺ signals essential for correct regulation of numerous cellular processes (1, 11, 27). We describe here an approach using TIRF microscopy to reveal the quantal substructure of elementary Ca²⁺ puffs arising from clusters of IP₃Rs by directly resolving the gating of individual channels. These signals likely reflect the activity of type 1 IP₃Rs, as this is reported to be the major (99%) isoform present in SH-SY5Y cells (28). An analogous quantal dissection was previously reported for the elementary Ca²⁺ sparks generated by arrays of RyRs in cardiac cells (29), but in that instance the quantal steps were inferred from differences in rate of rise of the fluorescence signal, and it was not possible to discern the kinetics of individual channels. The enhanced fidelity we describe probably arises from differences in imaging modality (TIRF vs. line-scan confocal microscopy), and because the longer duration of Ca²⁺ flux during puffs (≈100 ms) compared with sparks (≈10 ms) facilitates kinetic resolution. Our results indicate that local IP₃-mediated signals are highly variable events involving anywhere from 1 to >20 IP₃R channels, and that this variability arises both from heterogeneity between puff sites and between successive events at a given site. This functional architecture mirrors that of sparks, which recruit variable cohorts from as few as 1 to as many as 10 RyRs (29).

The rapid upstroke of puffs reflects fast recruitment of IP₃Rs within <20 ms after initiation (Fig. 5*D*). This coordination likely results from CICR evoked by the high local [Ca²⁺] in nanodomains around open channels clustered at the puff site. The latencies we observe are within the range (24 ms) obtained from electrophysiological recordings of single IP₃Rs following concentration jumps to saturating (300 μM) [Ca²⁺] (30), but a rigorous quantitative analysis will require further detailed information of IP₃R spacing and kinetics of Ca²⁺ binding and activation. For example, infrequent observations of multiple, discrete steps on the rising phase of puffs might reflect sites with unusually large spacing between IP₃Rs. In light of the rapid

PHYSIOLOGY

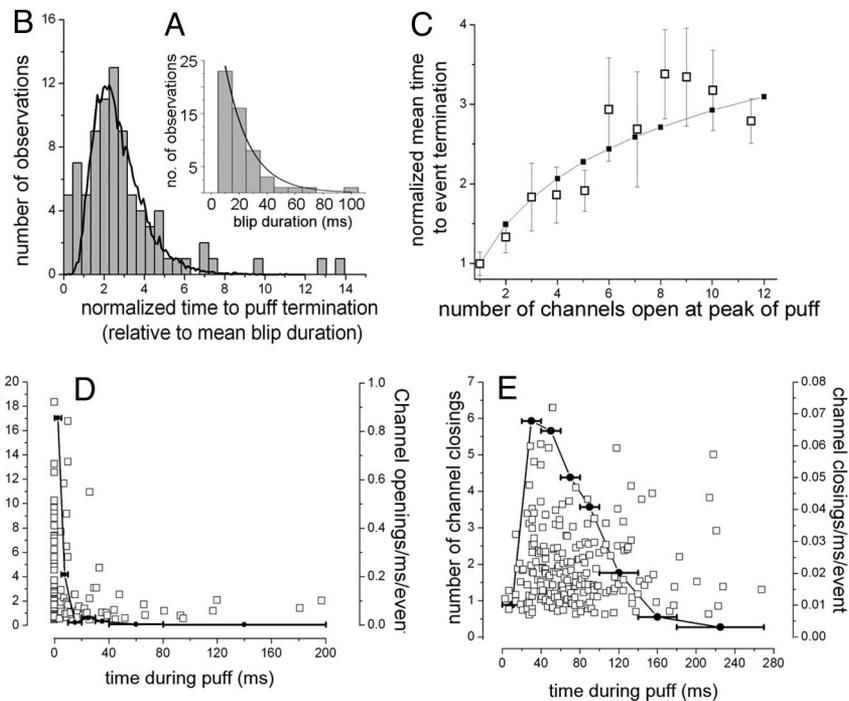**Fig. 5.** IP$_3$R channel gating kinetics during blips and puffs. (*A*) Distribution of unitary blip event durations, after excluding the small proportion of events with durations >100 ms. The curve is a single exponential with time constant τ of 17 ms. (*B*) Histogram shows the distribution of puff durations, measured as the interval between attainment of peak amplitude and return to baseline and expressed relative to the mean blip duration of 17 ms. Data were selected from events with normalized peak amplitudes between 5 and 10, and exclude events that showed channel openings during the falling phase. The black curve shows simulated data generated assuming that 8 channels are open at the peak of the puff, and then close stochastically and independently after a mean dwell time of 17 ms. (*C*) Mean time to event termination as a function of the estimated number of channels open at the peak. Open symbols are experimental data. Filled symbols show the relationship predicted if channels close stochastically and independently after a mean lifetime of 17 ms. (*D* and *E*) Graphs plot, respectively, the rates of channel openings/closings as functions of time after initiation of a puff. Symbols are individual measurements of numbers of channels that opened/closed during successive 5-ms time bins, estimated from the normalized fluorescence change during that interval (*Left*). Curves show the mean rates of channel opening/closing averaged over varying time bins (*Right*).

initial positive feedback, it is surprising that puffs are not stereotypical, all-or-none events, but rather show great variability such that, on average, only approximately half of the available IP$_3$R channels open (Fig. 4*D*). This is unlikely to result in stochastic recovery of IP$_3$R from an inactivated state induced by a preceding puff, because the mean size of the first puffs evoked by photo-released IP$_3$ is not appreciably greater than subsequent puffs (17), and puff amplitudes show only weak correlations with the amplitude of a preceding puff and with the inter-puff interval (31). Instead, we propose that the rapid cessation of channel openings results from an inhibitory process with kinetics comparable to the regenerative activation. The variability in puff amplitudes (peak number of open channels) at a given site may then reflect a stochastic interplay between activation and inactivation processes, such that an appreciable proportion of IP$_3$Rs become inactivated before they have a chance to open.

The mechanism of termination of puffs (and analogous sparks mediated by RyRs) is of great interest, because CICR is otherwise expected to prolong these events indefinitely (32, 33). Among several postulated mechanisms (33), our results rule out stochastic attrition (i.e., breakdown of CICR because all channels randomly happen to be closed at the same time) as the sole explanation, as this predicts that puff durations will increase exponentially with the number of open channels (30). Moreover, the step-wise decay of puffs at integer quantal levels indicates that termination results from channel gating and not simply because local exhaustion of ER Ca^{2+} stores diminishes the single-channel Ca^{2+} flux. Instead, the progressive closure of IP$_3$R channels after the peak of a puff, with relatively few subsequent openings, is consistent with the rapid onset of a

strong inhibitory process as discussed earlier. Our data do not directly address the nature of this inhibition, but a likely candidate is the strong Ca^{2+}-dependent inhibition exhibited by the type 1 IP$_3$R predominant in this cell type. Channels that are open at the peak of the puff subsequently close after a mean duration characteristic of the single-channel lifetime, and infrequent openings on the falling phase may reflect slow recovery of inactivated channels.

In conclusion, IP$_3$-mediated Ca^{2+} signals are an example in which stochastic fluctuations at the single-channel level give rise to whole-cell responses (11). Development of minimally invasive, functional single-channel imaging methods thus represents a major advance in elucidating the link between these nanoscopic and macroscopic cell signaling processes. By its nature, TIRF microscopy is likely to be limited to cultured or isolated cells in which the ER/sarcoplasmic reticulum is close to the cell membrane, and may thus be unable to fully reveal potential complexities of channel clustering and IP$_3$ gradients within native tissues. Nevertheless, our approach should be widely applicable to studies of the functional architecture and dynamics of intracellular ion channels in intact cells at the truly single-molecule level.

Materials and Methods

Cell Culture and Loading. Human neuroblastoma SH-SY5Y cells were cultured as previously described (17) in a mixture (1:1) of Ham's F12 medium and Eagle MEM, supplemented with 10% (vol./vol.) FCS and 1% nonessential amino acids. Cells were incubated at 37 °C in a humidified incubator gassed with 95% air and 5% CO$_2$, passaged every 7 days, and used for a maximum of 20 passages. Four days before imaging, cells were harvested in PBS solution without Ca^{2+} or Mg^{2+} and subcultured in Petri dishes with glass coverslips as

the base (MatTek) at a seeding density of 3×10^4 cells/mL. Cells were then loaded a few hours before use by incubation with Hepes-buffered saline solution (in mM: NaCl, 135; KCl, 5; MgSO$_4$, 1.2; CaCl$_2$, 2.5; Hepes 5; glucose, 10) containing 1 μM ci-IP$_3$/PM (SiChem) at room temperature for 45 min, followed by incubation with 1 μM caged ci-IP$_3$/PM plus 5 μM fluo-4 AM (Invitrogen) at room temperature for 45 min, and finally 45 min with 5 μM EGTA-AM (Invitrogen).

TIRF Microscopy. Imaging of changes in $[Ca^{2+}]_i$ was accomplished by using a home-built TIRF microscope system based around an Olympus IX 70 microscope equipped with an Olympus X60 TIRFM objective (NA 1.45). Fluorescence of cytosolic fluo-4 was excited within the $\approx$100-nm evanescent field formed by total internal reflection of a 488-nm laser beam incident through the microscope objective at the cover glass/aqueous interface. Images of emitted fluorescence ($\lambda > 510$ nm) were captured at a resolution of 128×128 pixels (1 pixel = 0.33 μm) at a rate of 420 frames s^{-1} by a Cascade 128 electron-multiplied CCD camera (Roper Scientific). Photo-release of i-IP$_3$ from a caged precursor was evoked by flashes of UV light (350–400 nm) derived from a fiber-optic arc lamp source introduced via a UV reflecting dichroic mirror in the upper side-port of the microscope. The UV light was adjusted to uniformly irradiate a region slightly larger than the imaging frame, and any given imaging field was exposed to only a single flash. We sought to obtain data under condition of roughly constant cytosolic [i-IP$_3$], and adjusted the flash duration as required between 50 and 400 ms so as to obtain a similar mean puff frequency ($\approx$1 per s/cell) in each cell to compensate for variations in loading of caged i-IP$_3$. We had previously shown that puff amplitude is relatively insensitive to increasing amounts of photo-released iIP$_3$, whereas puff frequency increases steeply (17).

Image Processing and Analysis. Image processing and analysis were done using MetaMorph 7.5 (Molecular Dynamics). After subtraction of the camera black offset level, image sequences were first processed by dividing each frame by an average of $\approx$100 frames captured before the photolysis flash, so that fluorescence represents a ratio ($\Delta F/F_0$) of the fluorescence change (ΔF) at each pixel relative to the mean resting fluorescence (F_0) before stimulation. The resulting image stack was then further processed by frame-by-frame subtraction of heavily smoothed (16×16 pixel low-pass filter) images, so as to correct for slow drift in basal fluorescence (16). Fluorescence traces like those in Fig. 2 were derived by measuring the average signal within 1×1 μm (3×3 pixel) regions of interest centered on visually identified Ca^{2+} release sites, identified as regions of repetitive localized increases in fluorescence. Super-resolution mapping of centroid positions of Ca^{2+} signals was accomplished adapting the FPALM program (provided by S. Hess, University of Maine, Orono, ME) to fit 2D Gaussian functions to the fluorescence images at individual sites. The graphical representation of puff activity in Fig. 1C was made using ImageJ (National Institutes of Health) to create a pseudo-colored image from an ASCII text file containing fluorescence measurements from 72 puff sites.

1. Berridge MJ, Lipp P, Bootman MD (2000) The versatility and universality of calcium signalling. *Nat Rev Mol Cell Biol* 1:11–21.
2. Berridge MJ (1997) Elementary and global aspects of calcium signalling. *J Physiol* 499:291–306.
3. Bootman M, Niggli E, Berridge M, Lipp P (1997) Imaging the hierarchical calcium signalling system in HeLa cells. *J Physiol* 499:307–314.
4. Bootman MD, Berridge MJ, Lipp P (1997) Cooking with calcium: the recipes for composing global signals from elementary events. *Cell* 91:367–373.
5. Thorn P, Lawrie AM, Smith PM, Gallacher DV, Petersen OH (1993) Local and global cytosolic calcium oscillations in exocrine cells evoked by agonists and inositol trisphosphate. *Cell* 74:661–668.
6. Yao Y, Choi J, Parker I (1995) Quantal puffs of intracellular calcium evoked by inositol trisphosphate in Xenopus oocytes. *J Physiol* 482:533–553.
7. Parker I, Yao Y (1996) Calcium transients associated with openings of inositol trisphosphate-gated channels in Xenopus oocytes. *J Physiol* 491:663–668.
8. Parker I, Yao Y (1991) Regenerative release of calcium from functionally discrete subcellular stores by inositol trisphosphate. *Proc R Soc London Ser B* 246:269–274.
9. Thomas D, et al. (2000) Microscopic properties of elementary calcium release sites in non-excitable cells. *Curr Biol* 10:8–15.
10. Rose HJ, Dargan S, Shuai J, Parker I (2006) 'Trigger' events precede calcium puffs in Xenopus oocytes. *Biophys J* 91:4024–4032.
11. Foskett JK, White C, Cheung KH, Mak DO (2007) Inositol trisphosphate receptor calcium release channels. *Physiol Rev* 87:593–658.
12. Bezprozvanny I, Watras J, Ehrlich BE (1991) Bell-shaped calcium-response curves of inositol trisphosphate- and calcium-gated channels from endoplasmic reticulum of cerebellum. *Nature* 351:751–754.
13. Parker I, Choi J, Yao Y (1996) Elementary events of inositol trisphosphate-induced calcium liberation in Xenopus oocytes: hot spots, puffs and blips. *Cell Calcium* 20:105–121.
14. Shuai J, Parker I (2005) Optical single-channel recording by imaging calcium flux through individual ion channels: theoretical considerations and limits to resolution. *Cell Calcium* 37:283–299.
15. Demuro A, Parker I (2004) Imaging the activity and localization of single voltage-gated calcium channels by total internal reflection fluorescence microscopy. *Biophys J* 86:3250–3259.
16. Demuro A, Parker I (2005) ''Optical patch-clamping'': single-channel recording by imaging calcium flux through individual muscle acetylcholine receptor channels. *J Gen Physiol* 126:179–192.
17. Smith IF, Wiltgen SM, Parker I (2009) Localization of puff sites adjacent to the plasma membrane: Functional and spatial characterization of calcium signaling in SH-SY5Y cells utilizing membrane-permeant caged inositol trisphosphate. *Cell Calcium* 45:65–76.

18. Callamaras N, Parker I (2000) Phasic characteristic of elementary calcium release sites underlies quantal responses to I inositol trisphosphate. *EMBO J* 19:3608–3617.
19. Dargan SL, Parker I (2003) Buffer kinetics shape the spatiotemporal patterns of inositol trisphosphate -evoked calcium signals. *J Physiol* 553:775–788.
20. Dakin K, Li WH (2007) Cell membrane permeable esters of D-myo-inositol 1,4,5-trisphosphate. *Cell Calcium* 42:291–301.
21. Riddoch FC, Rowbotham SE, Brown AM, Redfern CP, Cheek TR (2005) Release and sequestration of calcium by a caffeine- and ryanodine-sensitive store in a sub-population of human SH-SY5Y neuroblastoma cells. *Cell Calcium* 38:111–120.
22. Hille B (2001) *Ion Channels of Excitable Membranes* (Sinauer Associates, Sunderland, MA) 3rd Ed.
23. Del Castillo J, Katz B (1954) Quantal components of the end-plate potential. *J Physiol* 124:560–573.
24. Thul R, Falcke M (2004) Release currents of inositol trisphosphate receptor channel clusters and concentration profiles. *Biophys J* 86:2660–2673.
25. Shuai J, Pearson JE, Foskett JK, Mak DO, Parker I (2007) A kinetic model of single and clustered inositol trisphosphate receptors in the absence of calcium feedback. *Biophys J* 93:1151–1162.
26. Ionescu L, et al. (2007) Mode switching is the major mechanism of ligand regulation of inositol trisphosphate receptor calcium release channels. *J Gen Physiol* 130:631–645.
27. Callamaras N, Marchant JS, Sun XP, Parker I (1998) Activation and co-ordination of inositol trisphosphate -mediated elementary calcium events during global calcium signals in Xenopus oocytes. *J Physiol* 509:81–91.
28. Wojcikiewicz RJ (1995) Type I, II, and III inositol 1,4,5-trisphosphate receptors are unequally susceptible to down-regulation and are expressed in markedly different proportions in different cell types. *J Biol Chem* 270:11678–11683.
29. Wang SQ, Stern MD, Rios E, Cheng H (2004) The quantal nature of calcium sparks and in situ operation of the ryanodine receptor array in cardiac cells. *Proc Natl Acad Sci USA* 101:3979–3984.
30. Mak DO, et al. (2007) Rapid ligand-regulated gating kinetics of single inositol 1,4,5-trisphosphate receptor calcium release channels. *EMBO Rep* 8:1044–1051.
31. Fraiman D, Pando B, Dargan S, Parker I, Dawson SP (2006) Analysis of puff dynamics in oocytes: interdependence of puff amplitude and interpuff interval. *Biophys J* 90:3897–3907.
32. Groff JR, Smith GD (2008) Calcium-dependent inactivation and the dynamics of calcium puffs and sparks. *J Theor Biol* 253:483–499.
33. Stern MD, Cheng H (2004) Putting out the fire: what terminates calcium-induced calcium release in cardiac muscle? *Cell Calcium* 35:591–601.

PHYSIOLOGY